The role of structural transformations in magnetic behaviour of fluorosilicates of 3d transition metals

1997 J. Phys.: Condens. Matter 9 7161

(http://iopscience.iop.org/0953-8984/9/34/009)

J. Phys.: Condens. Matter **9** (1997) 7161–7171. Printed in the UK PII: S0953-8984(97)84882-5

The role of structural transformations in magnetic behaviour of fluorosilicates of 3d transition metals

S K Asadov†, K V Kamenev‡§, V I Kamenev†, B M Todris† and E A Zavadskii†

† Donetsk Physico-Technical Institute, National Academy of Sciences of Ukraine, 72 R Luxemburg Street, Donetsk 340114, Ukraine

‡ Department of Physics, University of Warwick, Coventry CV4 7AL, UK

Received 4 June 1997

Abstract. The stability of the structural phases in the fluorosilicate hexahydrates of some 3d transition metals $MSiF_6.6H_2O$ where M = Mn, Fe, Co and Ni is studied in a wide range of temperatures and pressures. The results are generalized in the form of a P–T phase diagram of crystal states. The triple points, new high-pressure phases and wide ranges of metastable states between them have been discovered. The correspondence between structural and magnetic P–T phase diagrams of the series is established.

1. Introduction

The fluorosilicate hexahydrates of divalent metals (M-FSH) with general formula $MSiF_6.6H_2O$ (M = Mn, Ni, Fe, and Co) have similar crystal structures, which can be described as a trigonally distorted CsCl-type lattice composed of $[SiF_6]^{2-}$ and $[M(H_2O)_6]^{2+}$. For the past thirty years these compounds have been a subject of numerous resonance, magnetic, optical, and structural studies due to the presence of thermally induced magnetic and structural transformations. According to the differences in lattice symmetry at room temperature (T_r) and low temperatures, the M-FSHs can be divided between three types. The first type is illustrated by Ni-FSH, which possesses $R\bar{3}$ structure in the entire temperature range studied [1]. Co-FSH belongs to the second type. Although at T_r it is also rhombohedral with the space group $R\bar{3}$, cooling below $T = 246$ K brings about a first-order phase transition [2, 3]. Comparison of the results described in [4] and [5] shows that the low-temperature phase of Co-FSH has monoclinic symmetry $P2_1/c$. For the fluorosilicates of Fe and Mn, belonging to the third type of behaviour, the mirror planes of symmetry parallel to the threefold axis are found at room temperature. Initially it was observed by means of diffraction measurements that Fe-FSH belongs to the $R\bar{3}m$ symmetry group [6] and Mn-FSH to $P\bar{3}m1$ [4]. More recently an x-ray study [7, 8] has revealed that there are some reflections incompatible with the $R\bar{3}m$ group. According to [7] and [8], these additional reflections allow an interpretation of this structure as a pseudo-hexagonal one based on a periodic alternation of the elements of monoclinic lattice $P2_1/c$. Nevertheless, in the present study we will identify the room-temperature phases as they are reported in [4] and [6]. The M-FSHs of this third type undergo a first-order phase transition to a low-temperature monoclinic $P2_1/c$ [5] state at 230 K for Mn-FSH and at 225 K for Fe-FSH.

§ Corresponding author. E-mail address: phsch@csv.warwick.ac.uk

0953-8984/97/347161+11$19.50

Besides the structural transformation mentioned above, there are phase transitions related to the changes in magnetic ordering at very low temperatures. Measurements at $T < 1$ K have shown that Ni-FSH is a ferromagnet while Mn- and Co-FSH are antiferromagnets with weak ferromagnetism. Study of these salts under pressure [9–11] suggests that the fluorosilicates of Co and Mn remain antiferromagnetic up to 40 and 80 MPa, respectively. Cooling at higher pressures brings about ferromagnetic ordering. Ni-FSH remains ferromagnetic in all pressures (up to 950 MPa), changing the type of magnetic anisotropy from 'easy axis' to 'easy plane' at 130 MPa. In Fe-FSH at $T < 7$ K two discontinuities induced by magnetic field at $H_1 = 9.8$ MA m^{-1} and $H_2 = 34.38$ MA m^{-1} [12] are found on the magnetization curve. These jumps disappear under pressure higher than 180 MPa and the magnetization smoothly increases with field [13].

The variety of structural transitions in M-FSHs as well as the changes in their magnetic properties under pressure described above became a reason for the study of these materials under hydrostatic compression. In the present paper we report the results of a comprehensive study of the influence of hydrostatic pressure on the stability of the crystalline states, on the temperature of phase transitions and on the mechanism for the phase transitions. From the results of this study, the P–T phase diagrams have been established; the triple points, new high-pressure phases and wide ranges of metastable states between them were discovered; the connections between the changes in crystalline structure and magnetic properties have been investigated.

2. Experimental details

The study has been carried out by two independent methods—differential thermal analysis (DTA) and x-ray diffraction, on single crystals grown from aqueous solutions by the method described in [14]. DTA was used to determine the temperatures of phase transitions and to characterize the thermal effects accompanying these transitions. A sample of M-FSH along with a reference material and a thermocouple was placed into the high-pressure cell which was also used as a furnace. The high-pressure cell made in the form of a beryllium-bronze cylinder was connected to a gas compressor by a steel capillary. Use of gaseous helium as a pressure-transmitting medium allowed us to carry out the measurements in isothermal as well as in isobaric conditions. Such a flexibility in the experimental setup has also enabled us to measure along any path in the P–T plane. The equipment employed has provided the possibility to conduct measurements in the range of temperatures of 12–300 K and pressures of 0–200 MPa within the accuracy of measurement of ± 0.5 K and ± 1.5 MPa, respectively.

The temperature and pressure dependences of interatomic distance d_{440} as well as the intensity and shape of the (440) reflection (the indexes are in the hexagonal axes of the rhombohedral lattice) in the M-FSH have been measured by means of x-ray diffraction. The ranges of stability of the different crystalline states on the P–T plane, the presence and type of phase transitions, and the values of temperature and pressure of the phase transitions have been determined according to the presence and the character of the anomalies on these dependences.

The (440) reflection was chosen for the convenience of the experiments. At first, this reflection can be registered from a natural face of the crystals. The high intensity of the reflection (about one hundred times higher than the intensity of the background) has allowed us to determine its position within an accuracy of $\pm 0.02^\circ$. This precision combined with the accuracy provided by the use of Cu K$\alpha_1 + \alpha_2$ radiation ($2\Theta_{440} \sim 80^\circ$) and complete standardization of the conditions of the x-ray experiments gave the overall accuracy of the determination of the interplane distance of d_{440} of $\pm 1.7 \times 10^{-2}$%. Secondly, the shape of

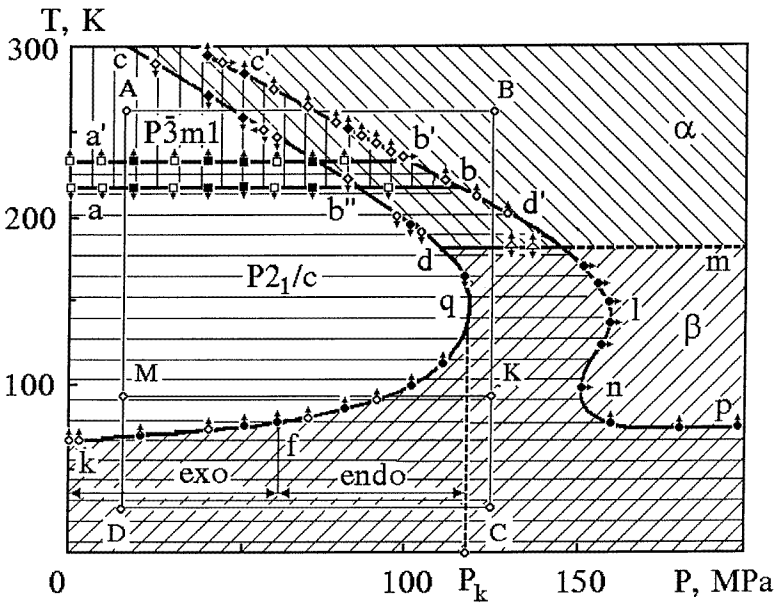

Figure 1. The P–T phase diagram of $MnSiF_6.6H_2O$.

the (440) reflection is sensitive to a loss of axis symmetry by the crystals.

For the x-ray study the high-pressure cell mounted on the DRON-3 diffractometer has been utilized. A single crystal was placed into the container made of beryllium and supported by a preheat-treated beryllium bronze bandage. The pressure (as it was the case of the DTA measurements) was induced with a gas membrane compressor. The complete description of the high-pressure cell can be found elsewhere [15]. The cell was designed to operate in the temperature region from 4.2 to 350 K and under pressures of up to 140 MPa.

3. Results and discussion

The results of the study are generalized in the form of the P–T phase diagrams for each of the studied M-FSHs which are all drawn in one style for convenience of comparison. The results obtained by the DTA method and the x-ray diffraction are marked with filled and open symbols, respectively. The arrows near the symbols indicate the directions of the change (increase or decrease) of the temperature or pressure when the anomalies were detected. The ranges of stability of the different phases are indicated by different shading.

3.1. Structural transformations in the fluorosilicate hexahydrate of manganese under pressure

The P–T phase diagram of Mn-FSH is presented in figure 1. The temperature of the phase transition between trigonal $P\bar{3}m1$ and monoclinic $P2_1/c$ phases observed at atmospheric pressure [4] is almost pressure independent in the entire region of existence for this transition, i.e. from ambient pressure to about 90 MPa.

An increase of temperature and/or pressure on the sample initially in the $P\bar{3}m1$ state leads to an abrupt decrease of d_{440} distance of about 1.6% as it crosses the bc' line. The

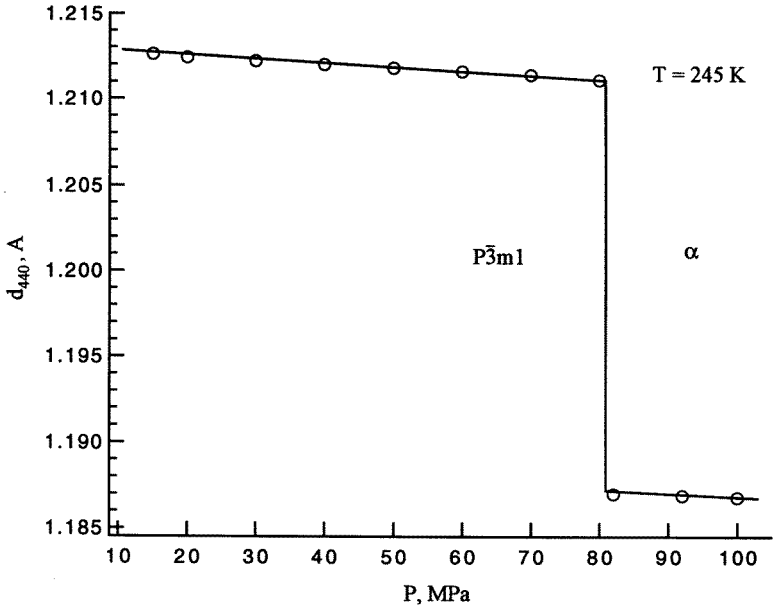

Figure 2. The pressure dependence of d_{440} in $MnSiF_6.6H_2O$ at $T = 245$ K.

typical pressure dependence of $d_{440}(P)$ is presented in figure 2. The abrupt change in d_{440} characterizes this phase transition as a first-order one. We assume that the sample remains trigonal in the new α-phase since the phase transition from $P\bar{3}m1$ to α is not accompanied by any change in the shape of the (440) diffraction peak. The negative slope of the bc' line indicates that the α-phase is both a high-pressure and a high-temperature phase with respect to the $P\bar{3}m1$ state. As temperature increases the sample undergoes the phase transition to α-phase as to the high-pressure phase, i.e. with a decrease in volume which is a rare phenomenon. The sample can either be returned to the phase $P\bar{3}m1$ by decreasing temperature and/or pressure (phase boundary $b''c$), or undergo a first-order phase transition to the state with $P2_1/c$ symmetry (phase boundary $b''d$). The reverse $P2_1/c \rightarrow \alpha$ phase transition takes place along the $b'd'$ line.

The triple point on the P–T diagram of $MnSiF_6.6H_2O$ is the crossing point of the following phase boundaries: $P\bar{3}m1 \leftrightarrow P2_1/c$, $P\bar{3}m1 \leftrightarrow \alpha$ and $\alpha \leftrightarrow P2_1/c$. As a result of the hysteretic character of the phase transitions, the triple point appears as b, b' and b'' for the transition from $P\bar{3}m1$, α and $P2_1/c$ states, respectively.

The phase $P2_1/c$ appears on cooling (phase boundary $ab''dq$) and remains in this low-temperature phase down to liquid helium temperature. The monoclinic phase does not appear in this sample, when cooling is carried out at pressures greater than $P_k = 120$ MPa. Instead, the sample shows an anomalous behaviour when crossing the dm line on the P–T phase diagram (figure 1). The anomaly appears as a break in the slope of the temperature dependence of d_{440} and is presented in figure 3 for two pressures both higher than P_k. The temperatures and pressures of the observed breaks form the dm line on the P–T phase diagram, which separates α and β states with higher and lower coefficients of thermal expansion along the [440] direction in the crystal lattice, respectively. Since on the dm line the thermal expansion coefficient changes abruptly while the interplane distance d_{440} does so continuously, then the $\alpha \leftrightarrow \beta$ transition can be classified as a second-order phase transition.

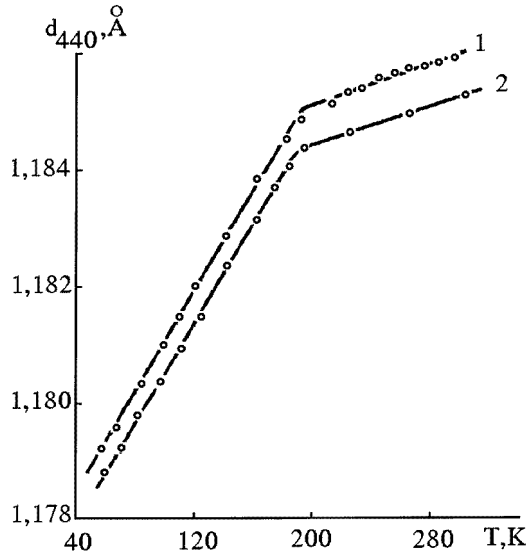

Figure 3. The temperature dependence of d_{440} in $MnSiF_6.6H_2O$ at different pressures: 1, $P = 130$ MPa; 2, $P = 135$ MPa.

Besides, the $\alpha \leftrightarrow \beta$ transition is not accompanied by any changes in the lineshape of the (440) reflection. This allows us to assume that the lattice in the β-state, as well as in the α-state, possesses a trigonal symmetry axis. Since the present x-ray study was limited to the pressures $P \leqslant 140$ MPa and the anomaly cannot be detected by means of DTA measurements, we can only suppose that the dm boundary will be maintained up to higher pressures.

The line $dqfk$ on the P–T diagram (figure 1) is the boundary of the first-order transition from the β to $P2_1/c$ state. To bring about the $\beta \rightarrow P2_1/c$ phase transition the sample should be brought to the range of absolute stability of $P2_1/c$ phase delineated by the $ab''dqfk$ boundary either by reducing pressure (along the KM line) or by a change of both pressure and temperature along the KCDM path. The transition to $P2_1/c$ is irreversible with respect to temperature since the sample remains monoclinic upon cooling to liquid helium temperature. To make the $\beta \rightarrow P2_1/c$ phase transition possible again it is necessary to cross the $a'b'bd'lnp$ boundary for the monoclinic state and bring the sample to the β-phase. The reverse $P2_1/c \rightarrow \beta$ transition can be directly realized along the $d'lnp$ boundary.

The lines of the appearance and disappearance of the different phases on the P–T diagram are separated by the metastable ranges marked with crossed hatching. Depending on the pre-history of the sample and its thermodynamic 'trajectory' on the diagram, any of the phases, which hatching covers the corresponding area of the diagram, can be realized in the sample. For example, only the $P\bar{3}m1 \rightarrow P2_1/c$ phase transition takes place on cooling along the AD path and the sample has monoclinic symmetry at the point D. However, when the sample is brought to the point D through $P\bar{3}m1 \rightarrow \alpha$ first-order and $\alpha \rightarrow \beta$ second-order phase transitions, leaving aside the boundary of appearance of $P2_1/c$ phase (for instance, along the ABCD path), then it will be in the β-phase with trigonal symmetry of the crystal lattice. Thus, the $P2_1/c$ and β-phases are metastable below the $pnld'dqfk$ line and remain relatively stable down to liquid helium temperature.

It is necessary to note that the thermal anomalies accompanying the first-order phase

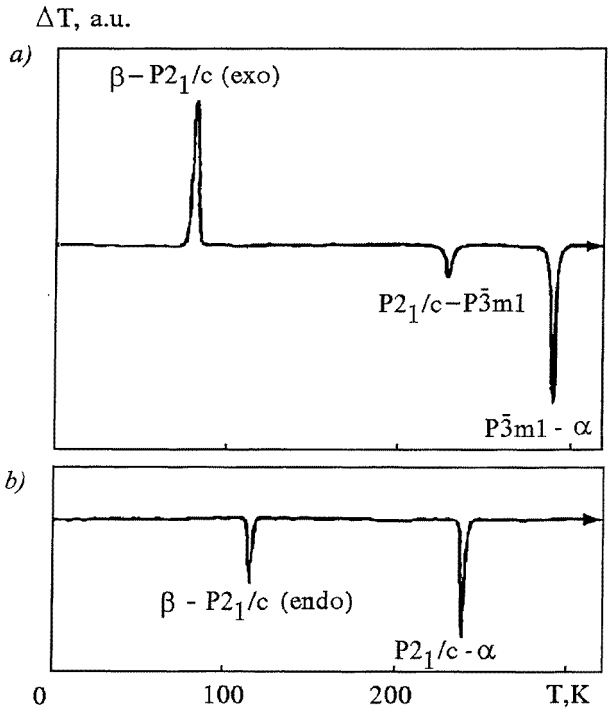

Figure 4. Thermograms (heating) obtained for $MnSiF_6.6H_2O$ at different pressures: (*a*) $P = 50$ MPa; (*b*) $P = 110$ MPa. The initial state is β.

transitions have a different sign along different sections of the phase boundaries of the monoclinic state. The heat absorption takes place on the $b'bd'l$ section of the phase boundary of the $P2_1/c$ phase, while along the lnp section of the same boundary the heat is released as the sample undergoes a phase transition to the β-phase. The development of the ordered $P2_1/c$ state from $P\bar{3}m1$ and the α-state on the sections $ab''d$ and $b''d$, respectively, is accompanied by heat release. The $\beta \rightarrow P2_1/c$ phase transition occurs as an endothermic transition (i.e. the heat is absorbed on heating) along the qf section of the boundary and as exothermic (i.e. the heat is released) along fk. The thermograms presented in figure 4 for different segments of the qfk boundary illustrate the behaviour typical for each of the corresponding segments. The irreversibility and exothermic character of the $\beta \rightarrow P2_1/c$ phase transition allow us to consider it as a relaxation process similar to crystallization of amorphous metals or as a transformation from a metastable state brought about by quenching to the most stable state on annealing.

3.2. Notable features of the P–T phase diagram of $FeSiF_6.6H_2O$

The phase diagram of $FeSiF_6.6H_2O$ is presented in figure 5 and reflects the following peculiarities in the behaviour of this compound under pressure.

(i) The $R\bar{3}m \rightarrow P2_1/c$ phase transition which was known to appear at ambient pressure [5] exists only to 7.5 MPa (the ab and $a'b'$ boundaries are for the direct and reverse transitions, respectively). The phase transition to the new state called the α-phase was found at pressures higher than 7.5 MPa. Since the intensity and the shape of the diffraction

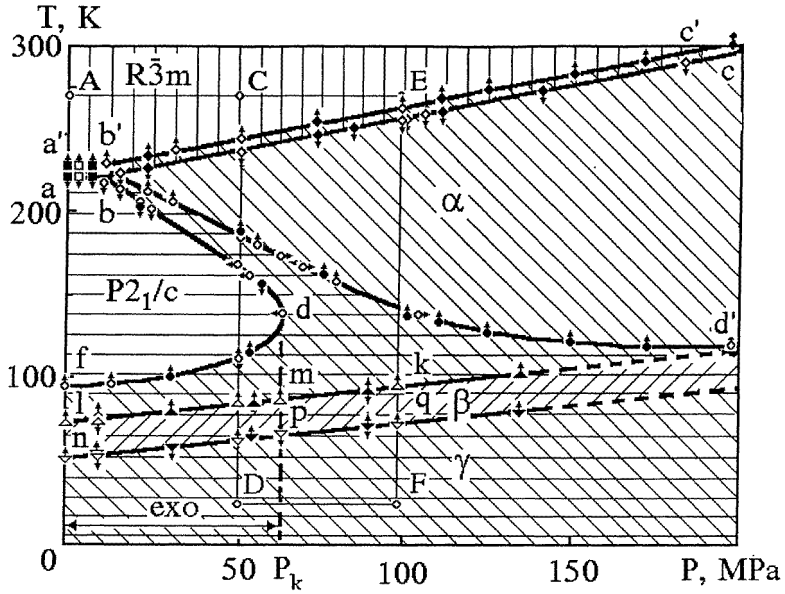

Figure 5. The P–T phase diagram of $FeSiF_6.6H_2O$.

maximum are unaffected by the phase transition we assume that the α-phase possesses a threefold symmetry axis.

(ii) Besides the $R\bar{3}m \rightarrow \alpha$ phase transition there is a first-order $\alpha \rightarrow P2_1/c$ phase transition occurring on cooling in the pressure region from 7.5 to 63 MPa. Below this transition the monoclinic structure remains stable down to liquid helium temperature.

(iii) The bc and bd lines of the direct $R\bar{3}m \rightarrow \alpha$ and $\alpha \rightarrow P2_1/c$ phase transitions, respectively, approach each other and the line of the $R\bar{3}m \rightarrow P2_1/c$ phase transition as pressure decreases and form a triple point b. The lines $b'c'$, $d'b'$ and $a'b'$ of the reverse phase transitions form triple point b'.

(iv) The $P2_1/c$ phase does not show up in the sample on cooling when $P > P_k$ ($P_k = 63$ MPa). Besides the $R\bar{3}m \rightarrow \alpha$, there are two second-order—$\alpha \rightarrow \beta$ and $\beta \rightarrow \gamma$—phase transitions taking place under pressures higher than P_k. The shape and intensity of the (440) peak remain the same in the β- and γ-phases, which allows us to assume that the β- and γ-phases as well as the α-phase possess threefold symmetry axes. The boundaries of β- and γ-phases at $P > P_k$ are outlined on the P–T phase diagram by the mk and pq lines, respectively.

(v) The lines of appearance and disappearance of $P2_1/c$ phase are delineated by the $abdf$ and $a'b'd'$ lines, respectively. The range between and below these two lines filled with crossed hatching indicates the area of metastability, where depending on the prehistory of the sample either $P2_1/c$ or α-, β- and γ-phases separated by the lines npq and lmk of second-order phase transitions can exist. If at the temperature T_k the sample of FeFSH is compressed isothermally to the pressures in the range 7.5 MPa < P < 63 MPa and then is cooled down isobarically (for example, along the ACD path on the P–T phase diagram), then the sample undergoes the phase transition from initial $R\bar{3}m$ state to the α-phase on the bc line and the $\alpha \rightarrow P2_1/c$ transition on the bd boundary. The boundaries fd, lmk and npq do not show up because of the metastable character of the

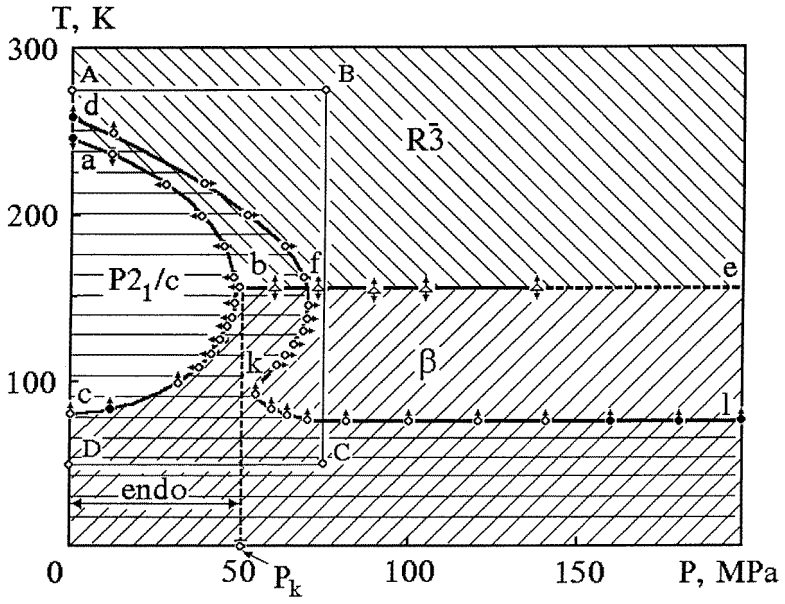

Figure 6. The P–T phase diagram of $CoSiF_6.6H_2O$.

α-, β- and γ-phases. Thus, the sample is in the $P2_1/c$ state at point D of the P–T phase diagram. Further heating along the DC path brings about the reverse sequence of the $P2_1/c \rightarrow \alpha \rightarrow R\bar{3}m$ phase transitions. If the sample is brought to the point D without entering the area of existence for the $P2_1/c$ phase (for example, along the ABFD path), then the sample undergoes a series of $R\bar{3}m \rightarrow \alpha \rightarrow \beta \rightarrow \gamma$ phase transitions and exists in the γ-phase at the D point. Heating along the DC path induces five sequential phase transitions—$\gamma \rightarrow \beta \rightarrow \alpha \rightarrow P2_1/c \rightarrow R\bar{3}m$.

(vi) Unlike the case of Mn-FSH, there is no change of sign on the thermal effect along the boundaries of appearance and disappearance of the monoclinic state in Fe-FSH. The $R\bar{3}m \rightarrow P2_1/c$, $\alpha \rightarrow P2_1/c$ and $\alpha \rightarrow P2_1/c$ phase transitions on the ab, bd and df lines, respectively, are accompanied by heat release. The reverse phase transitions taking place on the $a'b'$ and $b'd'$ lines are endothermic.

3.3. Phase transitions in $CoSiF_6.6H_2O$ under pressure

The following can be seen from the P–T diagram of $CoSiF_6.6H_2O$ presented in figure 6.

(i) The $R\bar{3} \rightarrow P2_1/c$ phase transition known at ambient pressure [1] exists only up to a pressure of $P_k = 50$ MPa. The pressure dependence of the phase transition forms the ab line on the diagram.

(ii) At pressures $P > P_k$ the sample undergoes a second-order phase transition detected by a break in slope of the isobaric dependence of $d_{440}(T)$. Since in the vicinity of the phase transition the shape and the intensity of the diffraction peak remain unchanged, we can assume that the new β-phase possesses a trigonal symmetry.

(iii) The monoclinic $P2_1/c$ phase can be reached on the P–T diagram not only by the first-order $R\bar{3} \rightarrow P2_1/c$ phase transition on cooling (the ab boundary) but also by the first-order $\beta \rightarrow P2_1/c$ phase transition on heating (the cb boundary). For the latter it

is necessary to bring the sample into the β-phase (point D) without entering the area of existence for the $P2_1/c$ phase (for example, along the ABCD path). Heating along the DA path induces two sequential first-order phase transitions $\beta \rightarrow P2_1/c \rightarrow R\bar{3}$ on crossing the lines bc and ab, respectively. The transition $\beta \rightarrow P2_1/c$ is irreversible with respect to temperature since cooling along the AD path brings about only the $R\bar{3} \rightarrow P2_1/c$ phase transition. The bc line does not show up and the sample remains of monoclinic symmetry down to the liquid helium temperatures. Thus, the range of appearance of the monoclinic phase is delineated by the abc boundary.

(iv) The boundary of disappearance of $P2_1/c$ phase is the $dfkl$ line. The range of metastable states is marked with the crossed hatching between the lines of the appearance (the abc line) and disappearance (the $dfkl$ line) of the monoclinic state. Depending on the pre-history of the sample on the diagram either $P2_1/c$ or $R\bar{3}$ and β-phase (separated by the bf line) appear in the sample in the metastable range.

(v) The change of the sign of the thermal effect is found on the boundaries of appearance and disappearance of the monoclinic state. The $R\bar{3} \rightarrow P2_1/c$ phase transition is exothermic along ab. The $\beta \rightarrow P2_1/c$ transition is also accompanied by heat release in the vicinity of the point b but at about 20 K below b the character of the transformation switches to endothermic. The reverse $P2_1/c \rightarrow \beta$ transition is accompanied by heat release along the lkf boundary and in the vicinity of the point f. The phase transition becomes endothermic again at about 12 K above f.

3.4. Anomalous temperature behaviour of the crystal lattice of $NiSiF_6.6H_2O$ under pressure

As pointed out in [1], at room temperature and ambient pressure Ni-FSH possesses the rhombohedral $R\bar{3}$ space symmetry group, which is preserved on cooling. Nevertheless, our results from the x-ray study show that there is an anomaly in the temperature behaviour of the crystal lattice, which shows up as a break in slope of the temperature dependence of d_{440} at 220 K. The appearance of the break is not accompanied by a change in the shape of symmetry-sensitive diffraction peak and is not seen on the DTA thermograms. The change in the slope of $d_{440}(T)$ indicates a continuous transition from the high-temperature state with lower value of the thermal expansion coefficient to the low-temperature state with its higher value. Formally, it is possible to conclude that the observed anomaly is a manifestation of a second-order phase transition from high-temperature $\alpha(R\bar{3})$- to isostructural low-temperature $\beta(R\bar{3})$-phase (the space symmetry of both phases is shown in brackets). The temperature of the $\alpha(R\bar{3}) \rightarrow \beta(R\bar{3})$ phase transition calculated from $d_{440}(T)$ for different pressures is almost pressure independent and forms the line cd on the P–T phase diagram of Ni-FSH (figure 7).

3.5. The correspondence of the structural and magnetic P–T phase diagrams

The presence of the critical pressure P_k on the structural P–T phase diagrams of Mn-FSH (figure 1), Fe-FSH (figure 5) and Co-FSH (figure 6) indicates that the samples of these M-FSHs being cooled down to low temperatures at $P < P_k$ would have a monoclinic $P2_1/c$ phase while cooling to the same temperatures under pressures P higher than P_k would bring about a rhombohedral $R\bar{3}$ ($P\bar{3}m1$, $R\bar{3}m$) symmetry for the lattice. This result is in good agreement with the previously established magnetic P–T phase diagram [10] according to which the magnetic ordering in Co-FSH and Mn-FSH at very low temperatures changes from anti-ferromagnetic when the samples are cooled at $P > P_k$ to ferromagnetic when the cooling occurs at pressures below P_k. Thus, we can assume that such a change in

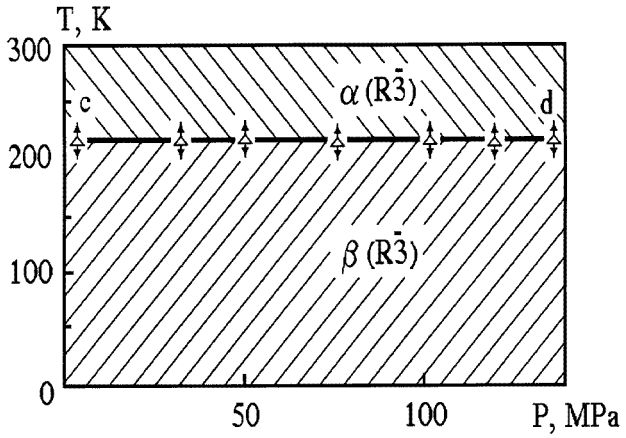

Figure 7. The P–T phase diagram of $NiSiF_6.6N_2O$.

magnetic ordering under pressure is a secondary effect with respect to the observed structural transformations, i.e. the antiferromagnetic ordering may be attributed to the $P2_1/c$ phase and the ferromagnetism to the $R\bar{3}$ phase. Similarly, in Fe-FSH cooling below 7 K at pressures lower than P_k with a magnetic field parallel to the threefold axis C_3 brings about a spin state with zero effective magnetic moment. In the same fields and temperatures but under pressures $P > P_k$ the disordered γ-phase of Fe-FSH loses its properties of an 'easy-axis' ferromagnet [13]. Finally, the P–T diagram of crystallographic states of Ni-FSH (figure 7) shows only one symmetry modification—$R\bar{3}$—for this fluorosilicate at very low temperatures. As a confirmation of the correspondence between structural and magnetic ordering in M-FSH described above, Ni-FSH orders only ferromagnetically at super-low temperatures in the whole range of applied pressures [11].

In conclusion, the effect of hydrostatic compression on the structural transformations in single-crystalline samples of fluorosilicate hexahydrates of divalent metals was studied by means of x-ray diffraction and differential thermal analysis. The results are summarized in the P–T diagram. The correspondence between structural and magnetic P–T phase diagrams of Mn-, Co- and Ni-FSH has been established.

Acknowledgment

This work was partly supported by Soros Program (ISSEP) grant No SPU062021.

References

[1] Ray S, Zalkin A and Templeton D 1973 *Acta Crystallogr.* B **29** 24 471
[2] Ray S 1964 *Indian J. Phys.* **38** 176
[3] Majumar M and Data S K 1965 *J. Chem. Phys.* **42** 418
[4] Kodera E, Torii A, Osaki K and Watanabe T 1972 *J. Phys. Soc. Japan* **32** 863
[5] Jehanno P and Varret F 1975 *Acta Crystallogr.* A **31** 857
[6] Hamilton W 1962 *Acta Crystallogr.* **15** 353
[7] Chevrier P and Jehanno G 1979 *Acta Crystallogr.* A **35** 912
[8] Chevrier P, Hardy A and Jehanno G 1981 *Acta Crystallogr.* A **37** 578
[9] Dyakonov V P, Zubov E E and Fita I M 1988 *25th All-Union Meeting on Low Temperature Physics (Leningrad, 1988)* Abstracts of Theses, part 2, p 110

[10] Dyakonov V P, Zubov E E and Fita I M 1988 *Fiz. Tverd. Tela* **30** 582
[11] Baryakhtar V G, Vitebsky I M, Galkin A A, Dyakonov V P, Fita I M and Tsintsadze G A 1983 *Zh. Eksp. Teor. Fiz.* **84** 1083
[12] Zavadskii E A, Todris B M, Zavorotnev Yu D and Asadov S K 1985 *Fiz. Nizkih Temp.* **11** 82
[13] Asadov S K, Zavadskii E A, Zavorotnev Yu D and Todris B M 1988 *Phys. Status Solidi* a **109** 307
[14] Kabanova N G, Lukin S N, Nejlo G N and Chernysh L F 1978 *Kristallografiya* **6** 1235
[15] Zavadskii E A, Zvada S S, Kamenev V I, Todris B M and Khartsev S I 1991 *Fiz. Tekh. Vysokih Davlenii* **1** 93